Stochastic Uncertainty Models for the Luminance Consistency Assumption

Thomas Corpetti and Etienne Mémin

***Abstract*—In this paper, a stochastic formulation of the brightness consistency used in many computer vision problems involving dynamic scenes (for instance, motion estimation or point tracking) is proposed. Usually, this model, which assumes that the luminance of a point is constant along its trajectory, is expressed in a differential form through the total derivative of the luminance function. This differential equation linearly links the point velocity to the spatial and temporal gradients of the luminance function. However, when dealing with images, the available information only holds at discrete time and on a discrete grid. In this paper, we formalize the image luminance as a continuous function transported by a flow known only up to some uncertainties related to such a discretization process. Relying on stochastic calculus, we define a formulation of the luminance function preservation in which these uncertainties are taken into account. From such a framework, it can be shown that the usual deterministic optical flow constraint equation corresponds to our stochastic evolution under some strong constraints. These constraints can be relaxed by imposing a weaker temporal assumption on the luminance function and also in introducing anisotropic intensity-based uncertainties. We also show that these uncertainties can be computed at each point of the image grid from the image data and hence provide meaningful information on the reliability of the motion estimates. To demonstrate the benefit of such a stochastic formulation of the brightness consistency assumption, we have considered a local least-squares motion estimator relying on this new constraint. This new motion estimator significantly improves the quality of the results.**

***Index Terms*—Image motion analysis, image quality, image sampling, stochastic processes.**

I. Introduction

MANY computer vision problems are formulated on the basis of the spatial and temporal variations of the image luminance. For instance, in all approaches requiring the tracking along time of points, curves, or surfaces [31], the evolution of the luminance function provides crucial information that can be used as a dynamic constraint [26], [27] or as an observation measurement [16], [21], [29]. In several domains where physical flows are involved (e.g., meteorology and oceanography), such an evolution law describes the transportation of physical scalar data f by motion field $\boldsymbol{v}$ under a global conservation constraint using the following classical relation:

$$\frac{df}{dt} = \frac{\partial f}{\partial t} + \boldsymbol{v} \cdot \boldsymbol{\nabla} f = 0 \tag{1}$$

where $\boldsymbol{\nabla}$ is the gradient operator in the x- and y-directions. When function f denotes the luminance function, this equation is referred to in computer vision as the optical flow constraint equation (OFCE) or the brightness consistency assumption and constitutes the only available information for motion estimation issues. Optical flow estimation has been intensively studied since the seminal work of Horn and Schunck [15], and a huge number of methods based on diverse variations of this constraint have been proposed in the literature [6], [11], [30], [32], [33]. Usually, a data model constructed from this constraint is associated with some spatial regularizers that promote motion fields with some spatial (and sometimes temporal) coherency. Many authors have proposed on this basis very efficient techniques. Readers can refer to [4]–[7], [18], [22]–[24], [28], [34], [35], and [37] for a nonexhaustive panel or to [14] for a recent review on estimators dedicated to fluid flows. Comparative performance evaluations of some of these techniques can be found in [2], [3], [12], and [14]. Among the developed approaches, the techniques focused first on the design of new regularization terms (able, for instance, to deal with occlusions and discontinuities or relying on physical grounds [10], [14]) and second on the application of advanced minimization strategies. Surprisingly, apart from some specific applications devoted to some specific types of imagery (e.g., fluid, biology, infrared imagery, tomography, and IRM), only a very few authors have worked on generic alternative data terms to the classical brightness consistency assumption, despite the fact that it plays a crucial role in the motion estimation process.

Moreover, the motion estimation issue should be seen in its most accomplished goal as a velocity or deformation metrology problem, in which one aims at recovering accurate motion measurements, and not only as a technique providing an approximate estimate of velocity vectors that inevitably give rise to erroneous drifts when integrated along time. Such drifts can be efficiently attenuated considering motion tracking procedures based on stochastic filtering [1] or optimal control [26]. These temporal integration approaches require the introduction of uncertainty models quantifying the reliability of the measurements. Accurate modeling of these uncertainties is crucial as large uncertainty values favor forecast motion values provided by the state variable dynamics, whereas small uncertainty values encourage high confidence in the measurements. In this paper, we aim at proposing a framework that allows us to estimate not only local motion measurements but

Manuscript received October 24, 2010; revised May 22, 2011; accepted June 23, 2011. Date of publication July 25, 2011; date of current version January 18, 2012. The associate editor coordinating the review of this manuscript and approving it for publication was Dr. Stefan Winkler.

T. Corpetti is with the Sino-French Laboratory on Computer Sciences, Automatics and Applied Mathematics (LIAMA), Institute of Automation, Chinese Academy of Sciences, Beijing 100190, China (e-mail: tcorpetti@gmail.com).

E. Mémin is with the Fluminance Group, National Institute for Research in Computer Science and Control (INRIA), 35042 Rennes, France (e-mail: memin@inria.fr).

Color versions of one or more of the figures in this paper are available online at http://ieeexplore.ieee.org.

Digital Object Identifier 10.1109/TIP.2011.2162742

also their uncertainties. To our knowledge, such uncertainty measurements are provided by none of the existing motion estimation techniques.

The conventional optical flow constraint relation (1) is in fact defined as the differential of a function known only on spatial and temporal discrete point positions (related to the image sequence spatiotemporal lattice). This is somewhat a strong constraint since, in practice, the grid points on which the luminance is defined is transported by a flow itself known only up to the same discrete positions. The result from this discretization process is an inherent uncertainty on the point location that can reveal to be of important magnitude when involving strong motions, large interframe lapse rate, or crude spatial discretization associated, for instance, with large spatial scale measurements. The idea is therefore to encode such a location uncertainty as a random variable and to incorporate the uncertainty transportation into the brightness consistency assumption. Stochastic calculus provides the differentiation rules needed to formalize such evolution law of uncertainty terms. In this paper, isotropic or anisotropic models of uncertainty have been settled, thus yielding to two different versions of a brightness assumption data model under a location uncertainty. Let us point out that such location uncertainty modeling allows us to propose a natural continuous multiscale estimation associated with a hierarchical discretization process on nested discrete lattices. Uncertainty model parameters are seen as additional parameters that have to be jointly estimated within the motion estimation procedure. The overall resulting scheme provides a proper way to measure in a joint way motion vectors and their associated uncertainty from the data. Our new models enable providing

1) a more accurate consistency conservation assumption equation that can be used in many computer vision problems;
2) an estimate of the motion uncertainties;
3) a natural continuous multiscale strategy for the motion estimation strategy.

We have the conviction that the association of an uncertainty measure to the estimated variable is of high importance in many applications. For instance, in the context of motion estimation, this uncertainty is directly related to the accuracy of the velocity field. For the tracking issue, such uncertainties are also linked to the confidence one may have in the conservation of any scalar field defined on the image grid. For a problem in which one aims at forecasting these scalar fields, the uncertainties enable simulating various configurations of the displaced scalar field image. This may have many practical applications (in geosciences in particular) when one wishes to predict scalar fields transported by the flow, such as temperature, pollutant sheets, or microorganism density.

In this paper, in order to validate our new data terms, we have designed a simple local motion estimator based on the principles of the Lucas–Kanade (LK) estimator [20]. We have used our new stochastic relations of the image luminance as an observation operator and compared it with the standard optical flow constraint (1). In addition, an original multiscale scheme, which is also interpreted as a stochastic uncertainty on the pixel grid, is presented and evaluated. Experiments are carried out on fluid particle images and on images of the Middleburry database. In the context of particle images, local approaches are currently used in operational systems. Those local techniques based on correlation have shown to be very efficient in this context. On particle images, dense motion estimation techniques may reach the same level of accuracy with a greater density of measurements when regularization terms reflecting well the physical properties of the fluid are considered [9], [10], [13], [38]. As for the second experiments, on several images issued from the Middleburry data set, we analyze the benefit of a data term based on the stochastic models proposed in this paper compared with a classical evolution based on (1). The experimentations indeed reveal better accuracy of the motion fields provided by our models, and we also highlight the benefit of the uncertainty maps extracted. Finally, we present the evaluation on the complete Middleburry database.

This paper is organized as follows: In Section II, we define a stochastic version of the luminance function by incorporating isotropic and anisotropic uncertainties. From this formulation, two conservation constraints of the image luminance are derived. If the velocity field is available or if we estimate it simultaneously, we propose in Section III a way to compute the associated uncertainty. Finally, Section IV presents a local multiscale LK motion estimator based on the brightness consistency stochastic models.

II. Stochastic Luminance Function and Conservation Constraints

A. Notations/Conventions

In this paper, we use four conventions/notations.

1) The image luminance is f.
2) We represent as a vector $\boldsymbol{X} = (\boldsymbol{X}^1, \ldots, \boldsymbol{X}^m)^T$ a grid of 2-D points, $\boldsymbol{X}^s \in \mathbb{R}^2$.
3) The "pixel" grid of images $\boldsymbol{X}_{t-1}$ is represented by the position of grid $\boldsymbol{X}$ at the initial time, set to $t-1$ [see Fig. 1(a)].
4) At time $t-1$, this grid is driven by velocity field $\boldsymbol{v}(\boldsymbol{X}_{t-1}, t-1) : \mathbb{R}^{2m} \times \mathbb{R}^+ \rightarrow \mathbb{R}^{2m}$ defined on initial grid $\boldsymbol{X}_{t-1}$ to generate new point positions $\boldsymbol{X}_t$ at time t [see Fig. 1(b)].

B. Stochastic Luminance Function

We first write the image luminance as a function of a stochastic process related to the position of image points. As illustrated in Fig. 1, if one assumes that velocity $\boldsymbol{v}$ to estimate transports the grid from $\boldsymbol{X}_{t-1}$ to $\boldsymbol{X}_t$ up to a Brownian motion, we can write

$$d\boldsymbol{X}_t = \boldsymbol{v}(\boldsymbol{X}_{t-1}, t-1)dt + \boldsymbol{\Sigma}(t, \boldsymbol{X}_t)d\mathbf{B}_t \tag{2}$$

where $\mathbf{B}_t = (\mathbf{B}_t^1, \ldots, \mathbf{B}_t^m)^T$ is a multidimensional standard Brownian motion of $\mathbb{R}^{2m}$, $\boldsymbol{\Sigma}$ is a $(2m \times 2m)$ covariance matrix, and $d\boldsymbol{X}_t = \boldsymbol{X}_t - \boldsymbol{X}_{t-1}$ represents the difference between the grid positions. Luminance function f usually defined on spatial points $\boldsymbol{x} = (x, y)$ at time t is here defined on the grid as a map from $\mathbb{R}^+ \times \mathbb{R}^{2m}$ into $\mathbb{R}^m$ and is assumed to be $C^{1,2}(\mathbb{R}^+, \mathbb{R}^{2m})$. Its differential is obtained following the differentiation rules of stochastic calculus (the so-called Itô formulas) that gives the

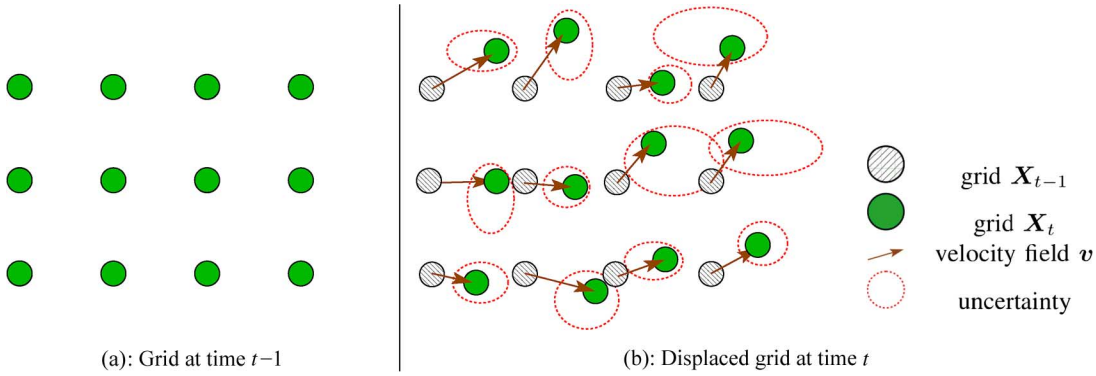

Fig. 1. Displacement of the grid of points. The initial grid at time $t-1$ in (a) is transported by velocity field $\boldsymbol{v}$ to reach the configuration at time t represented in (b), up to some uncertainties (dashed lines).

expression of the differential of any continuous function of an Itô diffusion of the form (2) (see [25] for an introduction to stochastic calculus), i.e.,

$$df(\boldsymbol{X}_t,t) = \frac{\partial f}{\partial t}dt + \sum_{i=(1,2)} \frac{\partial f(\boldsymbol{X}_t,t)}{\partial x_i} dX_t^i + \frac{1}{2} \sum_{(i,j)=(1,2)\times(1,2)} \frac{\partial^2 f(\boldsymbol{X}_t,t)}{\partial x_i \partial x_j} d\left\langle X_t^i, X_t^j \right\rangle. \quad (3)$$

The term $\langle X_t^i, X_t^j \rangle$ denotes the joint quadratic variations of X^i and X^j defined as the limit in probability, i.e.,

$$\left\langle X_t^i, X_t^j \right\rangle = \lim_{\delta t_k \to 0}^{\mathbb{P}} \sum_{t_k \leq t} \left(X_{t_{k-1}}^i - X_{t_k}^i \right) \left(X_{t_{k-1}}^j - X_{t_k}^j \right)$$

which can be computed according to the following rules:

$$\begin{aligned} \langle B^i, B^j \rangle &= \delta_{ij} t \\ \langle h(t), h(t) \rangle &= \left\langle h(t), dB^i \right\rangle = \left\langle B^j, h(t) \right\rangle = 0 \end{aligned} \quad (4)$$

where $\delta_{ij} = 1$ if $i = j$, $\delta_{ij} = 0$ otherwise, and $h(t)$ is a deterministic function. Compared with classical differential calculus, new terms related to the Brownian random terms have been introduced in this stochastic formulation. A possible way to represent the stochastic part of (2) is to use an isotropic uncertainty variance map $\sigma(X_t,t) : \mathbb{R}^+ \times \mathbb{R}^{2m} \to \mathbb{R}^m$, i.e.,

$$\boldsymbol{\Sigma}(\boldsymbol{X}_t,t) d\mathbf{B}_t = \text{diag}\left(\sigma(\boldsymbol{X}_t,t)\right) \otimes \mathbb{I}_2 d\mathbf{B}_t \quad (5)$$

where $\mathbb{I}_2$ is the (2×2) identity matrix, and $\otimes$ denotes the Kronecker product. Alternatively, one can use anisotropic intensity-based uncertainties along the normal (with variance σ_η) and the tangent (with variance σ_τ) of the photometric contour following

$$\boldsymbol{\Sigma}(\boldsymbol{X}_t,t) d\mathbf{B}_t = \text{diag}\left(\sigma_\eta(\boldsymbol{X}_t,t)\right) \otimes \boldsymbol{\eta} dB_t^\eta + \text{diag}\left(\sigma_\tau(\boldsymbol{X}_t,t)\right) \otimes \boldsymbol{\tau} dB_t^\tau. \quad (6)$$

Vectors

$$\boldsymbol{\eta} = \frac{1}{|\nabla f|} \begin{pmatrix} f_x \\ f_y \end{pmatrix} \quad \boldsymbol{\tau} = \frac{1}{|\nabla f|} \begin{pmatrix} -f_y \\ f_x \end{pmatrix}$$

represent the normal and tangent of the photometric isolines, respectively, and B^η and B^τ are two scalar independent multidimensional Brownian noises of $\mathbb{R}^m$ and $f_\bullet = \partial f(X_t,t)/\partial \bullet$ for $\bullet = (x,y)$. Let us now express luminance variations $df(X_t,t)$ under such isotropic or anisotropic uncertainties.

1) Isotropic Uncertainties: Applying Itô formula (3) to the isotropic uncertainty model yields a luminance variation, which is defined as

$$df(\boldsymbol{X}_t,t) = \left(\frac{\partial f}{\partial t} + \nabla f \cdot \boldsymbol{v} + \frac{1}{2}\sigma^2 \Delta f \right) dt + \sigma \nabla f \cdot d\boldsymbol{B}_t. \quad (7)$$

2) Anisotropic Uncertainties: Considering the anisotropic uncertainty model (6), the corresponding quadratic variations are

$$d\left\langle \boldsymbol{X}_t^1, \boldsymbol{X}_t^1 \right\rangle = \frac{1}{|\nabla f|^2} \left(\sigma_\eta^2 f_x^2 + \sigma_\tau^2 f_y^2 \right) dt \quad (8)$$

$$d\left\langle \boldsymbol{X}_t^2, \boldsymbol{X}_t^2 \right\rangle = \frac{1}{|\nabla f|^2} \left(\sigma_\eta^2 f_y^2 + \sigma_\tau^2 f_x^2 \right) dt \quad (9)$$

$$d\left\langle \boldsymbol{X}_t^1, \boldsymbol{X}_t^2 \right\rangle = \frac{1}{|\nabla f|^2} (f_x f_y) \left(\sigma_\eta^2 - \sigma_\tau^2 \right) dt \quad (10)$$

and variation of luminance df is now

$$\begin{aligned} df(\boldsymbol{X}_t,t) &= \left(\frac{\partial f}{\partial t} + \nabla f \cdot \boldsymbol{v} + \frac{\nabla f^T \nabla^2 f \nabla f}{2|\nabla f|^2} \left(\sigma_\eta^2 - \sigma_\tau^2 \right) + \frac{\sigma_\tau^2 \Delta f}{2} \right) dt \\ &\quad + \sigma_\eta \|\nabla f\| dB_t^\eta + \underbrace{\sigma_\tau \nabla f^T \boldsymbol{\tau} dB_t^\tau}_{=0}. \end{aligned} \quad (11)$$

In this brightness variation model, the stochastic term related to the uncertainty along the tangent vanishes (since the projection of the gradient along the level lines is null).

It is straightforward to remark that the standard brightness consistency assumption is obtained from (7) or (11) using zero uncertainties ($\sigma = \sigma_\eta = \sigma_\tau = 0$). The proposed stochastic formulation thus enables using a softer constraint. From this formulation, let us now derive generic models for the evolution of the image luminance transported by a velocity field with a location uncertainty.

C. Uncertainty Models for Luminance Conservation

Starting from a known grid $\boldsymbol{X}_{t-1}$ and its corresponding velocity, the conservation of the image luminance can be quite naturally expressed from conditional expectation $\mathbb{E}(df(\boldsymbol{X}_t,t)|\boldsymbol{X}_{t-1})$ between $t-1$ and t. To compute this term, we exploit the fact (as shown in the Appendix) that the expectation of any function $\Psi(\boldsymbol{X}_t,t)$ of stochastic process $d\boldsymbol{X}_t$ [as in (2)] knowing grid $\boldsymbol{X}_{t-1}$ is

$$\mathbb{E}\left(\Psi(\boldsymbol{X}_t,t)\,|\boldsymbol{X}_{t-1}\right)=\Psi(\boldsymbol{X}_{t-1}+\boldsymbol{v},t)*\mathcal{N}(0,\boldsymbol{\Sigma}) \tag{12}$$

where $\mathcal{N}(0,\boldsymbol{\Sigma})$ is a multidimensional centered Gaussian. This latter relation indicates that the expectation of function $\Psi(\boldsymbol{X}_t,t)$ knowing location $\boldsymbol{X}_{t-1}$ under a Brownian uncertainty of variance $\boldsymbol{\Sigma}$ is obtained by a convolution of $\Psi(\boldsymbol{X}_{t-1}+\boldsymbol{v},t)$ with a centered Gaussian kernel of variance $\boldsymbol{\Sigma}$.

Assuming that $\boldsymbol{\Sigma}$ is known, our new luminance variation model $\mathbb{E}(df(\boldsymbol{X}_t,t)|\boldsymbol{X}_{t-1})$ is hence defined as

$$\begin{aligned}\mathbb{E}\left(df(\boldsymbol{X}_t,t)|\boldsymbol{X}_{t-1}\right)&=g_{\boldsymbol{\Sigma}}*\left(df(\boldsymbol{X}_{t-1}+\boldsymbol{v},t)\right)\\&=g_{\boldsymbol{\Sigma}}*\mathcal{H}(f,\boldsymbol{v})dt\end{aligned} \tag{13}$$

where function $\mathcal{H}(f,\boldsymbol{v})$ corresponds to the bounded variation part of the luminance differential. Its form depends on the type of uncertainty considered. For an isotropic diffusion, the expectation of this function is

$$\mathbb{E}\left(\mathcal{H}(f,\boldsymbol{v})|\boldsymbol{X}_{t-1}\right)=g_\sigma*\left(\boldsymbol{\nabla}f\cdot\boldsymbol{v}+\frac{\partial f}{\partial t}+\underbrace{\frac{1}{2}\sigma^2\Delta f}_{\mathcal{F}(f)}\right) \tag{14}$$

whereas for the anisotropic version, it is

$$\begin{aligned}\mathbb{E}\left(\mathcal{H}(f,\boldsymbol{v})|\boldsymbol{X}_{t-1}\right)=&g_{\boldsymbol{\Sigma}}\\&*\left(\boldsymbol{\nabla}f\cdot\boldsymbol{v}+\frac{\partial f}{\partial t}+\underbrace{\frac{\boldsymbol{\nabla}f^T\boldsymbol{\nabla}^2f\boldsymbol{\nabla}f}{2|\boldsymbol{\nabla}f|^2}\left(\sigma_\eta^2-\sigma_\tau^2\right)+\frac{\sigma_\tau^2\Delta f}{2}}_{\mathcal{F}(f)}\right).\end{aligned} \tag{15}$$

If the brightness conservation constraint strictly holds, one obtains $\sigma=\sigma_\eta=\sigma_\tau=0$; the Gaussian kernels turn to Dirac distributions, and relations (13)–(15) correspond to (1). The proposed model thus brings a natural extension of the usual brightness consistency data model. Furthermore, as a bounded variation process, $\mathcal{H}(f,\boldsymbol{v})$ has a null quadratic variation, i.e.,

$$\mathbb{E}\left(\mathcal{H}^2(f,\boldsymbol{v})\right)=g_{\boldsymbol{\Sigma}}*\mathcal{H}^2(f,\boldsymbol{v})=0. \tag{16}$$

An approximation of this relation for a locally constant velocity in space will provide us a local least-squares estimation scheme for the unknown velocity. Before presenting this procedure, in the next section, we propose a way to estimate uncertainties σ_η and σ_τ.

III. Uncertainty Estimation

Assuming that an observed motion field $\boldsymbol{v}_{\text{obs}}$ that transports the luminance is available (we will describe in Section IV a local technique for this estimation), it is possible to estimate uncertainties $\sigma_\eta(\boldsymbol{x},t)$ and $\sigma_\tau(\boldsymbol{x},t)$ for each location $\boldsymbol{x}$ at time t.

A. Estimation of σ_η

Computing the quadratic variation of luminance function df between $t-1$ and t using the properties in (4) yields

$$d\left\langle f(\boldsymbol{X}_t,t),f(\boldsymbol{X}_t,t)\right\rangle=\sigma_\eta^2(\boldsymbol{X}_t,t)\left\|\boldsymbol{\nabla}f(\boldsymbol{X}_t,t))\right\|^2 \tag{17}$$

for the isotropic or anisotropic version, where $\sigma=\sigma_\eta$ in the isotropic formulation. This quadratic variation can be also approximated from luminance f by

$$d\left\langle f(\boldsymbol{X}_t,t),f(\boldsymbol{X}_t,t)\right\rangle\approx\left(f(\boldsymbol{X}_t,t)-f(\boldsymbol{X}_{t-1},t-1)\right)^2. \tag{18}$$

As convergence in probability implies convergence in distribution, the conditional expectation of both previous terms should be identical, and one can estimate the variance by

$$\sigma_\eta(\boldsymbol{X}_t)=\sqrt{\frac{\mathbb{E}\left(f(\boldsymbol{X}_t,t)-f(\boldsymbol{X}_{t-1},t-1)\right)^2}{\mathbb{E}\left(\left\|\boldsymbol{\nabla}f(\boldsymbol{X}_t,t))\right\|^2\right)}}. \tag{19}$$

The expectations in the numerator and the denominator are then computed at displaced point $X_{t-1}+\boldsymbol{v}_{\text{obs}}(\boldsymbol{X}_{t-1})$ through the convolution of variance $\boldsymbol{\Sigma}(\boldsymbol{X}_{t-1},t-1)$. A recursive estimation process thus emerges from (19). Let us note that this recursion corresponds to the following least-squares estimation:

$$\sigma_\eta^2=\arg\min_\sigma\left[\mathbb{E}df^2(\boldsymbol{X}_t,t)-\sigma^2\mathbb{E}\left\|\boldsymbol{\nabla}f(\boldsymbol{X}_t,t))\right\|^2\right]^2 \tag{20}$$

where $df^2(\boldsymbol{X}_t,t)$ is a shortcut notation for quadratic variation $d\langle f(\boldsymbol{X}_t,t),f(\boldsymbol{X}_t,t)\rangle$. This provides us a simple scheme for the estimation of the uncertainty directed along the isophotometric curves' normals. However, in the case of an anisotropic noise model, the uncertainty along the tangent is also needed.

B. Estimation of σ_τ

It is not possible to estimate the uncertainty along the photometric contours in a similar way since, as shown in (11), this quantity does not appear in the noise associated with the luminance variation and, therefore, is not involved in the corresponding quadratic variations. Writing the Itô diffusion associated with the velocity projected along the tangent yields

$$\boldsymbol{v}_{\text{obs}}^T\boldsymbol{\tau}=\boldsymbol{v}(\boldsymbol{X}_{t-1},t-1)^T\boldsymbol{\tau}dt+\sigma_\tau(t,\boldsymbol{X}_t)dB_t^\tau. \tag{21}$$

This scalar product constitutes a scalar Gaussian random field of mean $\mu=\boldsymbol{v}(\boldsymbol{X}_{t-1},t-1)^T\boldsymbol{\tau}$ (assuming $\boldsymbol{v}(\boldsymbol{x},t)$ is a bounded variation process) and covariance $(\text{diag}(\sigma_\tau))$. We assume that

scalar product $\boldsymbol{v}^T\boldsymbol{\tau}$ and tangent uncertainty $\sigma_\tau(t,\boldsymbol{x})$ are sufficiently smooth in space and can be well approximated, respectively, by the local empirical mean and variance over a local spatial neighborhood $N(\boldsymbol{x})$ of point $\boldsymbol{x}$. That is

$$\mu = \frac{1}{|N(\boldsymbol{x})|}\sum_{\boldsymbol{x}_i\in N(\boldsymbol{x})}\left(\boldsymbol{v}_{\text{obs}}(\boldsymbol{x}_i,t-1)^T\boldsymbol{\tau}\right) \tag{22}$$

$$\sigma_\tau^2 = \frac{1}{|N(\boldsymbol{x})|-1}\sum_{\boldsymbol{x}_i\in N(\boldsymbol{x})}(\boldsymbol{v}_{\text{obs}}(\boldsymbol{x}_i,t-1)^T\boldsymbol{\tau}-\mu)^2. \tag{23}$$

Relations (14) and (15) provide new models for the variation of the image luminance under isotropic or anisotropic uncertainties. Here, we have presented a technique to estimate such uncertainties from an available velocity field. The next section focuses on the application of those extended brightness consistency models for motion estimation.

IV. Application of the Proposed Luminance Models

This section aims at defining a simple local motion estimator that embeds the proposed evolution models as an observation term. As previously indicated, the quadratic variation of the bounded variation term of the luminance function is null. We thus have

$$\mathbb{E}\left(\mathcal{H}^2(f,\boldsymbol{v})\right) = g_{\boldsymbol{\Sigma}} * \mathcal{H}^2(f,\boldsymbol{v}) = 0. \tag{24}$$

As the classical OFCE based on (1), an observation model based on this constraint is ill posed. Similarly to the well-known LK estimator, we cope with this difficulty by assuming a constant flow within a Gaussian windowing function defined by the uncertainty estimate. However, for a small uncertainty, this model will be likely to be still subject to the aperture problem. We introduce, hence, an additional uncertainty isotropic function of variance σ^ℓ, which defines the minimal windowing function at which the estimation is performed. As a result of the locally spatially constant approximation of the motion field, constraint (24) can only be approached; we thus seek to fulfill it in the least-squares sense. Sought motion estimate $\boldsymbol{v}$ should thus minimize

$$\min_{\boldsymbol{v}} g_{\sigma^\ell} * g_{\boldsymbol{\Sigma}} * \left(\boldsymbol{\nabla} f\cdot\boldsymbol{v} + \frac{\partial f}{\partial t} + \mathcal{F}(f)\right)^2 \tag{25}$$

which yields the following relation for any position $\boldsymbol{x}$:

$$\left(g_{\sigma^\ell} * g_{\boldsymbol{\Sigma}} * \begin{bmatrix} f_x^2 & f_xf_y \\ f_xf_y & f_y^2 \end{bmatrix}\right)\boldsymbol{v} = -g_{\sigma^\ell} * g_{\boldsymbol{\Sigma}} * (\mathcal{F}(f)+f_t)\begin{bmatrix} f_x \\ f_y \end{bmatrix}. \tag{26}$$

Let us note that, in our model, the Gaussian windowing function can be interpreted as the distribution of a new isotropic constant uncertainty term related to the grid resolution and independent of the motion uncertainties depending on the image data. In practice, the choice of convolution kernel σ^ℓ is crucial: a large value of σ^ℓ will remove all details, whereas a small value is likely to be unstable and may lead to an extreme case of an ill-posed problem. In addition, such motion estimation procedure, which is based on a linearized version of the displaced frame difference, leads to inaccurate measurements of large displacements when the linear assumption of the brightness consistency breaks (high photometric gradients and/or large displacements). To prevent such limitations, many authors have proposed to embed such estimation procedures within a pyramidal setup. However, a pyramidal representation requires Gaussian filtering, sampling, and interpolation of the input data, which is likely to introduce artifacts that spoil the estimation. Interpreting the windowing function convolution as associated with the computation of the expectation of a grid uncertainty random term will allow us to define an original continuous multiresolution framework. This is presented in the next section.

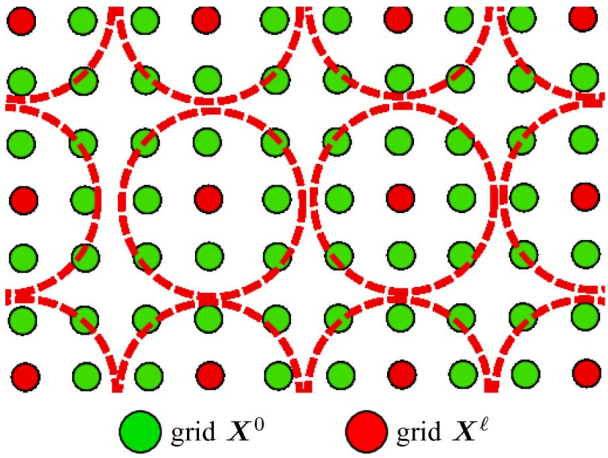

Fig. 2. Multiresolution grids represented through an isotropic Brownian process. Clear circles: original pixel grid. Dark circles: grid at a given resolution ℓ.

1) Multiresolution: A multiresolution scheme consists of redefining the problem on grid $\boldsymbol{X}^\ell$, which can be viewed as a coarse representation of initial grid $\boldsymbol{X}^0 = \boldsymbol{X}$ with a Brownian isotropic uncertainty of constant variance σ^ℓ. This is illustrated in Fig. 2: From initial pixel grid $\boldsymbol{X}^0 = \boldsymbol{X}$ that corresponds to the plain circles, the problem is redefined on grid $\boldsymbol{X}^\ell$ (represented by the dotted circles), which is a coarse representation of $\boldsymbol{X}$. This reads

$$\boldsymbol{X}^\ell = \boldsymbol{X}^0 + \sigma^\ell \mathbb{I}_2 d\mathbf{B}. \tag{27}$$

Motion $\boldsymbol{v}(\boldsymbol{X}^\ell_{t-1}, t-1)$ on this grid should minimize expectation $E(\mathcal{H}^2(f,\boldsymbol{v})|\boldsymbol{X}^0)$, which is equivalent (see the Appendix) to a convolution of $\mathcal{H}^2(f,\boldsymbol{v})$ with isotropic Gaussian $\mathcal{N}(O,\sigma^\ell)$. Therefore, one exactly gets the system in (25), which is locally solved by inverting the system in (26). A main advantage of such a formulation of the multiresolution setup is to naturally get rid of the use of a pyramidal image representation. Instead of dealing with successive decimations of factor 2 of the initial image to fix the different multiresolution levels, the evolutions of levels ℓ are much flexible here. This framework may be interpreted as a scale-space representation of the extended brightness consistency assumption [19]. However, in our case, it rigorously stems from an uncertainty analysis of the point location.

TABLE I
QUANTITATIVE COMPARISONS OF THE DNS SEQUENCE WITH A PYRAMIDAL LK (LK, [20]), A COMMERCIAL TECHNIQUE BASED ON CORRELATION (COM, LA VISION SYSTEM), HORN AND SCHUNCK (HS, [15]), TWO FLUID-DEDICATED MOTION ESTIMATORS WITH DIV-CURL SMOOTHING TERMS (DC1 [10] AND DC2 [38]), A FLUID-DEDICATED MOTION ESTIMATOR WITH TURBULENCE SUBGRID MODELS IN THE DATA TERM (TUR, [8]), OUR APPROACH USING THE CLASSICAL OFCE (OFCE), AND OUR APPROACH IN ISOTROPIC (ISO) AND ANISOTROPIC (ANISO)

	LK	COM	HS	DC 1	DC 2	TUR	OFCE ($57s$)	ISO ($63s$)	ANISO ($81s$)
AAE	6.07^o	4.58^o	4.27^o	4.35^o	3.04^o	4.49^o	4.53^o	3.59^o	3.12^o
RMSE	0.1699	0.1520	0.1385	0.1340	0.09602	0.1490	0.1243	0.1072	0.0961

With all these elements, we can define the incremental local motion estimation technique presented in the next section.

2) Incremental Framework: The local estimator proposed here comprises a specific multiresolution scheme where, at each level, an incremental framework is defined to estimate as accurately as possible the uncertainties. The incremental algorithm is used.

Incremental Algorithm

1) Initializations:
   - Fix an initial resolution level $\ell = L$
   - Define $\tilde{f}(X_{t-1}, t) := f(X_{t-1}, t)$; $\boldsymbol{v} = 0$;
2) Estimation for level ℓ
   a) Initializations:
      - $n = 1$; $\boldsymbol{v}^0 = 0$;
      - Fix a normal uncertainty σ_η^0
      - Fix a tangent uncertainty σ_τ^0 (if anisotropic formulation)
   b) Estimate σ_η^n by relation (19)
   c) Estimate σ_τ^n by measuring the tangential uncertainty of $\boldsymbol{v}$ [see (23)]
   d) Find $\boldsymbol{v}^n$ by local inversions of system (26)
   e) Update motion field: $\boldsymbol{v} := \boldsymbol{v} + \boldsymbol{v}^n$
   f) Warp image $f(X_t, t)$: $\tilde{f}(X_{t-1}) = f(X_{t-1} + \boldsymbol{v}, t)$
   g) $n := n + 1$
   h) **Loop** to step b until convergence ($|\boldsymbol{v}^n| < \epsilon$);
3) Decrease the multiresolution level: $\sigma^\ell = \lambda \sigma^\ell$
4) **Loop** to step 2 until convergence ($\sigma^\ell < \sigma^\ell_{\min}$).

The previous framework is a natural and simple implementation of a local motion estimation technique using the proposed models for the evolution of the luminance. A quantitative and qualitative evaluation of such an estimator, in comparison with the classical OFCE, will be presented in Section V.

V. EXPERIMENTAL RESULTS

We present here some experimental results of the local motion estimator described in Section IV. We show examples on synthetic fluid images and on the Middleburry database.[1] It is important to outline that the estimator defined in Section IV constitutes a local technique whose aim is simply to validate, compare, and qualify the observation model based on stochastic uncertainties versus the usual OFCE (1). Hence, its performances have to be compared with other local approaches.

[1]http://vision.middlebury.edu/flow/.

Following the proposed algorithm, four uncertainty parameters have to be set, i.e., σ_η^0 and σ_τ^0 (initial values of the uncertainties), σ^ℓ (coarse-scale level), and $\sigma^\ell_{\min}$ (finest scale level). In practice, we have fixed $\sigma_\eta^1 = \sigma_\tau = 1$, $\sigma^\ell = 40$, and $\sigma^\ell_{\min} = 7$. As for the multiscale setup, parameter λ that rules the scale decrease ($\sigma^{\ell+1} = \lambda\sigma^\ell, \sigma^{\ell+1} > \sigma^\ell_{\min}$) has been set to $\lambda = 0.3$. We can note that a standard pyramidal scheme would correspond to $\lambda = 0.5$. In practice, we have found, as in [36], that smaller values were more efficient. This will be illustrated in the next section. As a first benchmark, we analyze the results obtained on images depicting the evolution of a 2-D turbulent fluid flow.

A. Fluid Images

In fluid imagery, it is common to visualize and analyze flows with particles: the fluid flow is seeded with small particles and enlightens through a laser sheet. All existing commercial systems are local motion estimators based on correlation techniques. These technique are usually referred to as particle image velocimetry (PIV) methods.

We used a pair of synthetic images of 256×256 pixels obtained by direct numerical simulation (DNS) of Navier–Stokes equations and representing a 2-D turbulent flow. Numerical values of the average angular error (AAE) [3] and the root-mean-square error (RMSE) are used as criteria to compare our estimators (isotropic and anisotropic) with some of the state-of-the-art approaches. These results are depicted in Table I. The techniques to which the proposed estimators are compared with are given as follows:

1) Horn and Schunck estimator (HS technique) [15];
2) commercial software based on correlation (DaVis 7.2 from LaVision GmbH; COM technique);
3) pyramidal incremental implementation of the LK estimator (LK technique) [20];
4) proposed framework in Section IV with the OFCE as an observation model (i.e., with a zero uncertainty; OFCE technique);
5) two fluid-dedicated dense motion estimators based on Div–Curl smoothing with different minimization strategies (DC1 and DC2 techniques) [10], [38];
6) fluid-dedicated dense motion estimator based on a turbulence subgrid model in the data term (TUR technique) [8].

The pyramidal LK implementation only differs from the multiscale estimator with zero uncertainty (OFCE) in the setting of the decreasing scale parameter to $\lambda = 0.5$. For techniques issued from our local framework (OFCE, ISO, and ANISO), we have added the run-time experiments. The estimation was performed using MATLAB on a 4-GB random access memory personal computer of 2.6 GHz. As for running times, it turns out, as expected, that the anisotropic version is longer. This is due to the

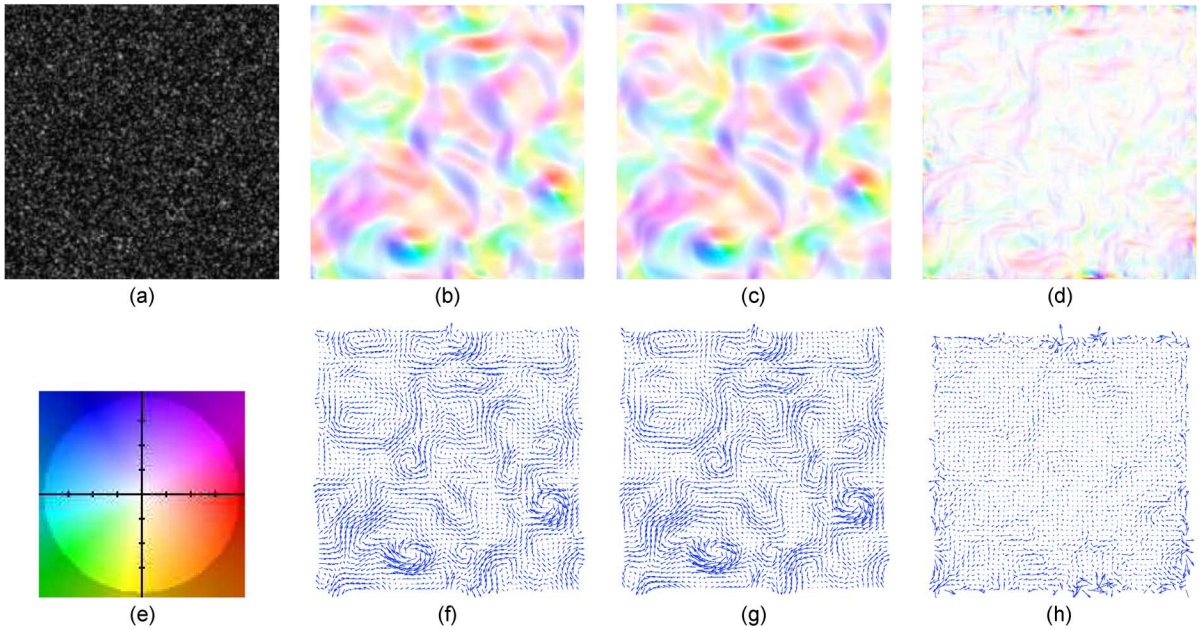

Fig. 3. Results on the DNS sequence. (Top) (a) Image of the sequence. (b) Estimated flow. (c) Real flow. (d) Difference flow represented with the coding color in (i). (Bottom) (e) Coding color for vector flow representation. (f)–(h) Vector representation of the estimated motion field, the ground truth, and the difference field, respectively ($\times 25$).

local convolutions (with various standard deviations) required by the technique that cannot be as efficiently implemented as an isotropic convolution with a constant standard deviation. However, it is very important to outline that this technique is local, and therefore, at each iteration, all local estimations (step 2d of the algorithm) can be parallelized.

In Fig. 3, we present an image of the sequence, the estimated flow with the proposed method (anisotropic version), and the error flow field. We have also plotted in Fig. 5 the velocity spectra of the different techniques and compared them with the ground truth. These spectra are represented in log–log coordinates [see Fig. 5(a)] and a standard–log coordinate system [see Fig. 5(b)] in order to highlight the accuracy of small and large scales, respectively.

In Table I, one can immediately observe that, compared with the other local approaches, our method provides very good results since the global accuracy is highly superior than the LK technique and the commercial software (COM technique). Compared with dense techniques (HS, DC1, and DC2), our numerical results are of the same order of magnitude, which is a very relevant point. They are competitive with some dense estimation techniques dedicated to fluid flow analysis (DC1 and DC2) [10], [38]. The comparison between the results OFCE, ISO, and ANI is very interesting since it highlights the benefit of the stochastic formulation of the image luminance. These three results have been estimated with the same incremental estimation framework of Section IV but using an observation model based on the usual OFCE [(1), OFCE technique], an isotropic uncertainty [(14), ISO technique], and an anisotropic uncertainty [(15), ANISO technique]. From the corresponding quantitative errors, it is obvious that the uncertainty modeling greatly improves the results, particularly in the anisotropic approach, but with a higher computational cost.

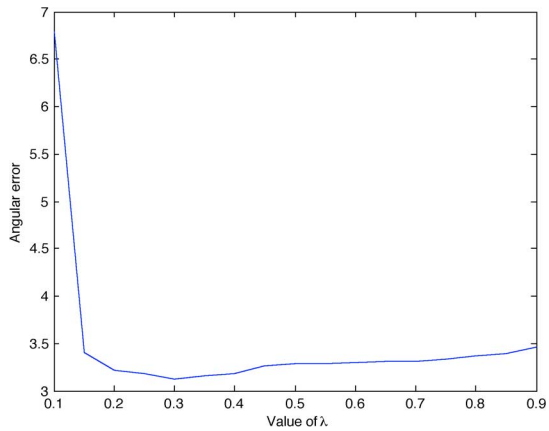

Fig. 4. Influence of decreasing parameter λ on the multiresolution process. Results of the angular error obtained for different values of λ using the ANI algorithm on the DNS sequence.

In order to evaluate the influence of decreasing parameter λ on the multiresolution process (step 3 of the incremental algorithm), we have plotted in Fig. 4 the angular error obtained on this pair of images with the ANI algorithm depending on several values of $\lambda \in [0.1, 0.9]$. As one can observe, the minimum is reached for $\lambda \approx 0.3$ and not around $\lambda = 0.5$, which corresponds to the usual pyramidal framework. The same observations hold for other kinds of images.

Now, if one observes the spectra of the velocity shown in Fig. 5, we see that the small scales (right part of the graph) are much better recovered by the proposed estimators than by the dense estimators. They are generally difficult to estimate and often smoothed out with the spatial regularizers introduced in the dense techniques. Even if the LK technique seems to exhibit better results on small scales, when observing Fig. 5(b),

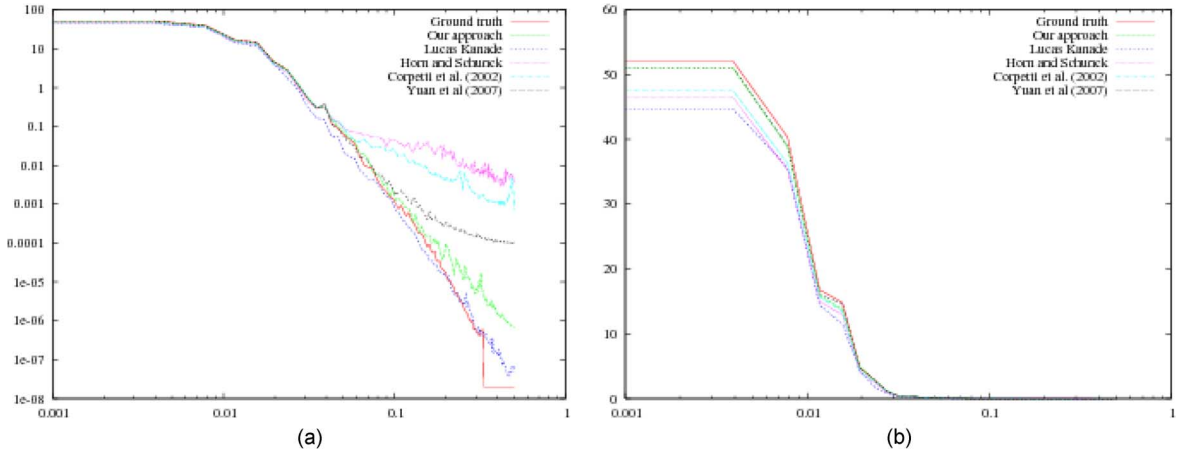

Fig. 5. Spectra of the velocity compared with the ground truth and for several methods. (a) Log–log representation (highlights small scales on the right part). (b) Nonlog–log representation (highlights large scales on the left part). Red: ground truth. Green: our approach (anisotropic version). Blue: LK [20]. Purple: Horn and Schunck [15]. Cyan: Div–Curl smoothing [10]. Black: Div–Curl in mimetic discretization [38].

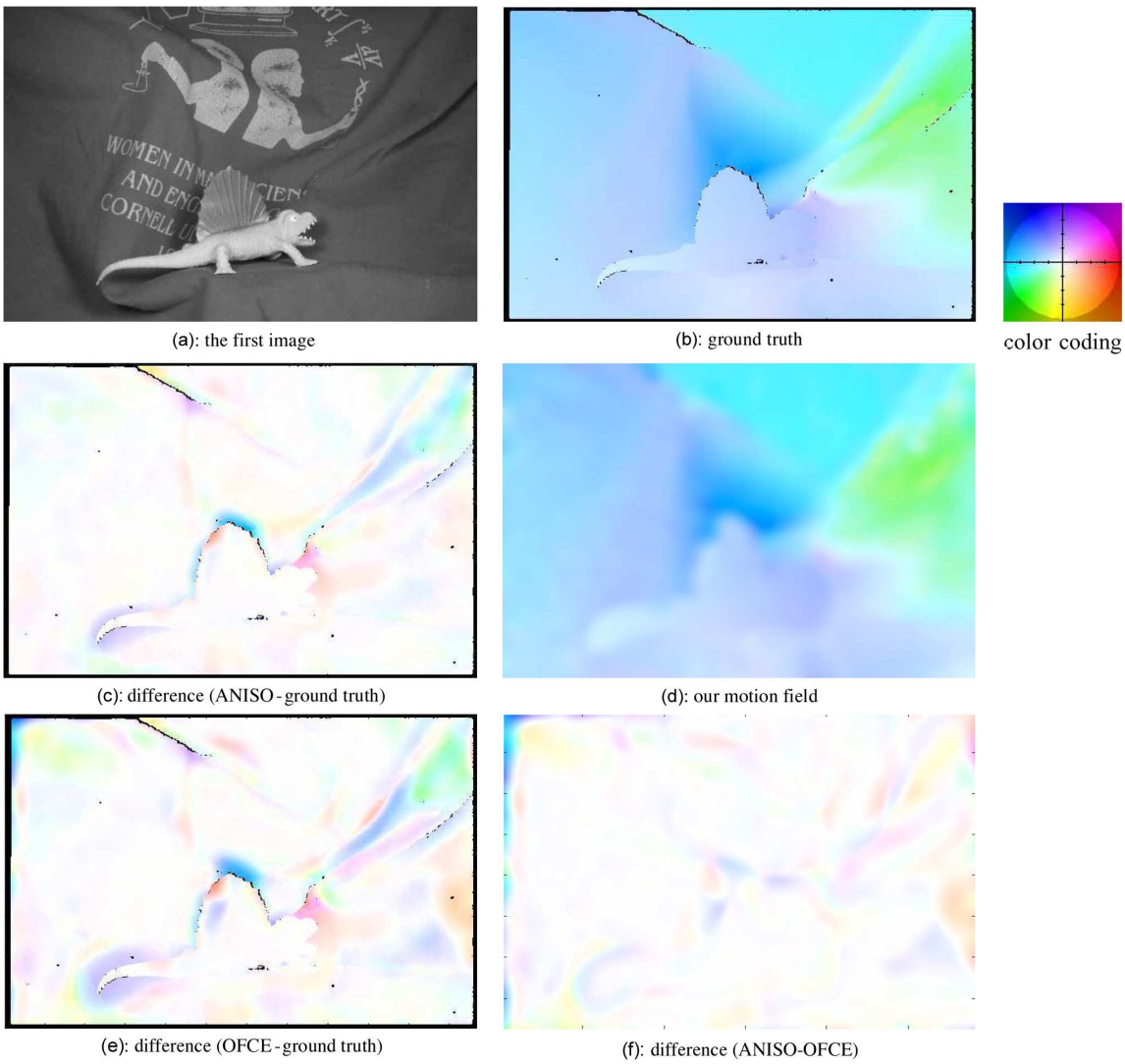

Fig. 6. Dimetrodon sequence. (a) Image of the sequence. (b) Ground truth. (c) Difference between the estimated velocity field and the ground truth. (d) Estimated motion field with our approach in the anisotropic version (ANISO). (e) Difference (OFCE–ground truth). (f) Difference (ANISO–OFCE).

it is obvious to note that large scales are badly estimated with this approach, and this yields very poor overall accuracy (see Table I). As for the large scales, the results are comparable with the best dense dedicated techniques. Hence, we believe that our

TABLE II
QUANTITATIVE RESULTS, TIME COMPUTATION, AND COMPARISONS OF THE DIMETRODON, YOSEMITE, AND VENUS SEQUENCES

Results on the Dimetrodon sequence (584×388 pixels)

Method	OFCE (124s)	ISO (208s)	ANISO (271s)	Bruhn et al.	Black, Anandan	Pyramid LK	Media Player^{TM}	Zitnick et al
Ang. error	7.95^o	3.95^o	$\mathbf{2.85}^o$	10.99^o	9.26^o	10.27^o	15.82^o	30.10^o

Results on the Venus sequence (420×380 pixels)

Method	OFCE (93s)	ISO (156s)	ANISO (197s)	Bruhn et al.	Black, Anandan	Pyramid LK	Media Player^{TM}	Zitnick et al
Ang. error	12.02^o	10.23^o	8.42^o	8.73^o	$\mathbf{7.64^o}$	14.61^o	15.48^o	11.42^o

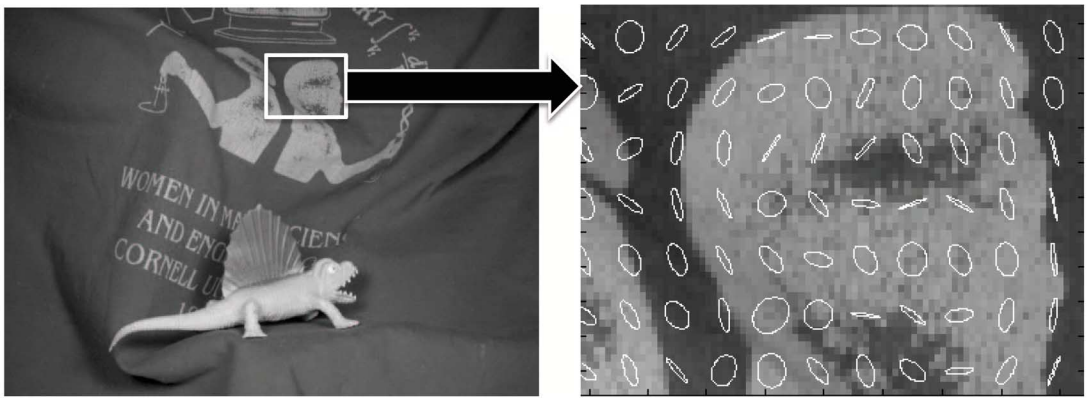

(a): representation of some uncertainty areas

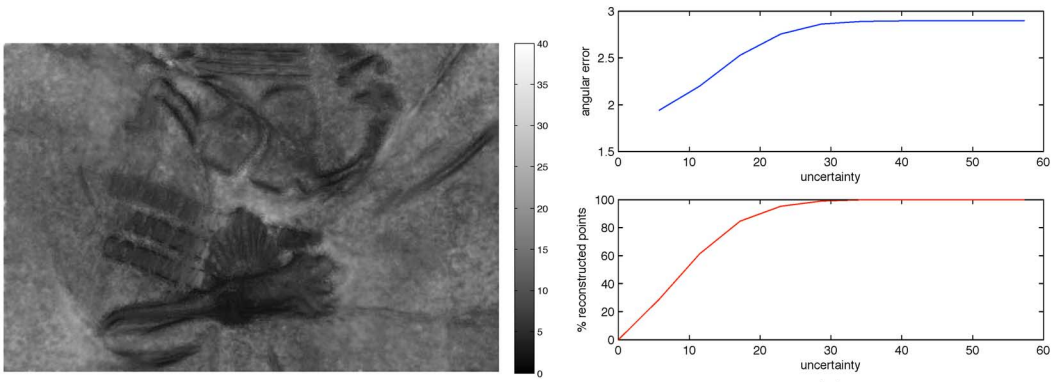

(b); uncertainty map (c)

Fig. 7. Uncertainty areas for the Dimetrodon sequence. (a) Snapshot of some anisotropic uncertainty areas highlighted by the ANISO technique, in which one can observe that the optical flow is computed depending on the photometric level lines of the luminance. (b) Extracted uncertainty map σ_η. (c) Evolution of the error and percentage of correct motion fields when one takes into account only velocity fields with smaller values of $\sqrt{\sigma_\eta^2 + \sigma_\tau^2}$.

estimator constitutes an appealing alternative to usual local PIV methods. Let us now describe the accuracy of the observation term on some images of the Middleburry database.

B. Middleburry Database

The Middleburry database has been recently proposed in [2] to compare recent and state-of-the-art optical flow methods. It contains several sequences with various challenging situations such as hidden textures, complex scenes, nonrigid motions, and high motion discontinuities. The aims of this validation are given here.

1) To highlight the benefit of the proposed brightness consistency model under a location uncertainty. To that end, we compare the results obtained with the simple motion estimator presented in the previous section using three observation terms, namely, the proposed ones in their isotropic and anisotropic versions and the usual OFCE (i.e., without uncertainty).
2) To promote the interest of the associated maps of uncertainties by demonstrating that they are directly related to the quality of the estimated motion field. To that end, we analyze the evolution of the error on the motion field when this latter is computed on points corresponding to low values of uncertainties.

On this database, we have first detailed the algorithm on a pair of images where the ground truth is available (since we need to compare the results on sparse motion fields). In order to help the reader in understanding the approach, in a second step, we have applied the technique on the whole database (even if the aim is to propose an alternative observation model only).

Evaluation of data with the ground truth: We have tested our approaches on the "Dimetrodon" and "Venus" sequences. For these sequences, the ground truth and a comparison with other state-of-the-art approaches are available. One image of each sequence is depicted in Figs. 6 and 8(a) with the associated ground truth in Figs. 6 and 8(b). The first sequence exhibits large homogeneous motions with variously located

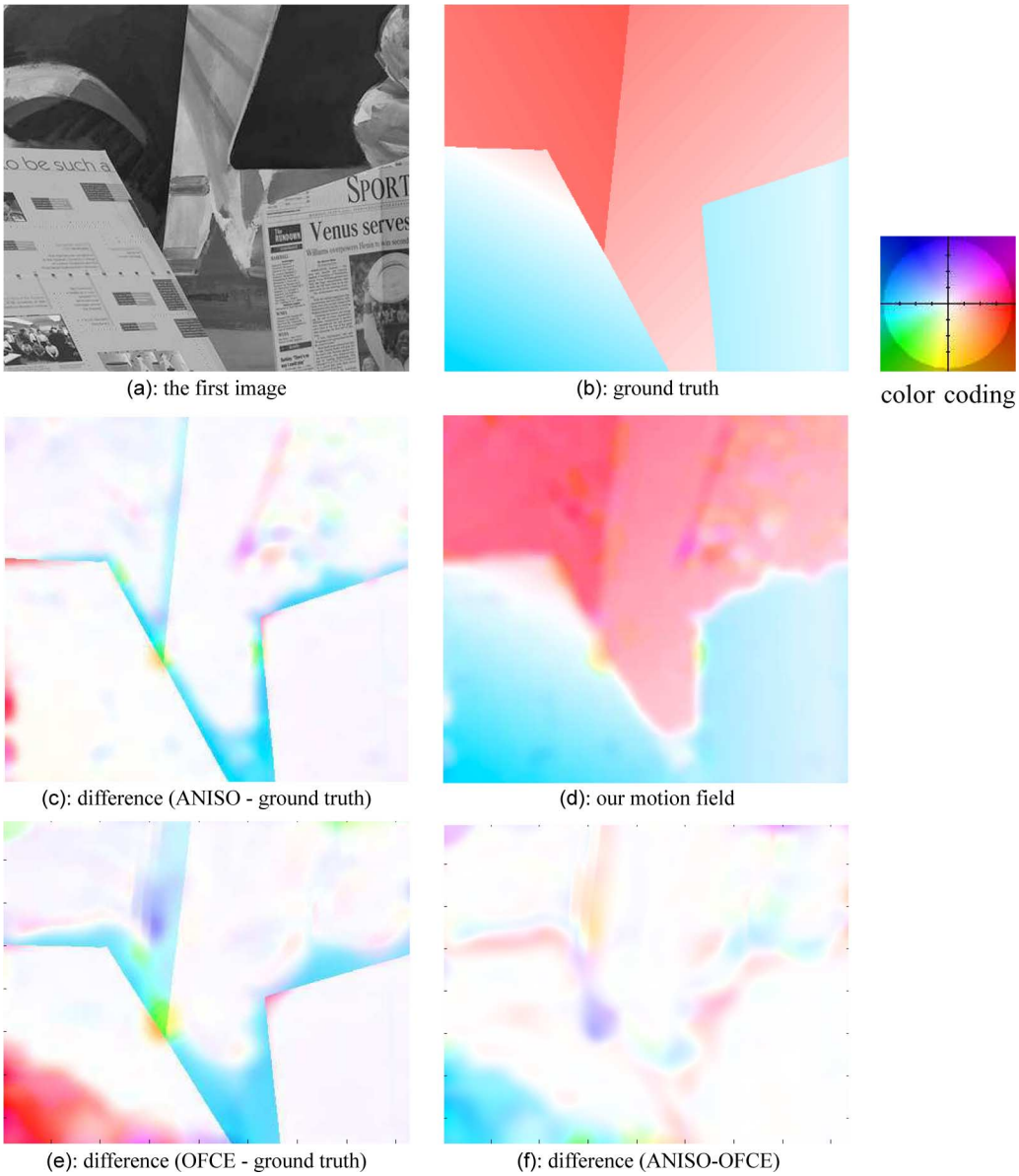

Fig. 8. Venus sequence. (a) Image of the sequence. (b) Ground truth. (c) Difference between the estimated velocity field and the ground truth. (d) Estimated motion field with our approach in the anisotropic version (ANISO). (e) Difference (OFCE–ground truth). (f) Difference (ANISO–OFCE).

discontinuities (around the dinosaur), whereas the discontinuities of the Venus sequence are more spatially homogeneous.

The quantitative results and associated run times are presented in Table II. When comparing the first three columns that use exactly the same technique but based on the usual OFCE [see (1)] and our luminance model with isotropic [ISO, see (14)] and anisotropic [ANISO, see (15)] uncertainties, it immediately points out that the proposed models enable enhancing significantly the quality of the results. This fair comparison of the three observation models onto the same estimator promotes the use of a stochastic formulation under anisotropic uncertainties. In fact, this latter version is a softer constraint than that of the OFCE, which, as previously shown, implicitly assumes a perfect measurement without any incertitudes. This better efficiency results in a larger time computation. However, as already mentioned, such local estimator can efficiently be implemented using parallel software.

The estimated motion fields under the anisotropic luminance formulation are represented in Figs. 6(d) and 8(d) and can be compared with the ground truth in Figs. 6(c) and 8(c).

The benefit of this new formulation of the luminance (ANISO version) compared with the usual brightness consistency assumption (OFCE version) is quantitatively demonstrated in Table II. In order to visually interpret these improvements, we have depicted in Figs. 6(e) and (f) and 8(e) and (f) the difference in motion fields between the OFCE estimator and the ground truth [see Figs. 6–8(e)] and the difference between ANISO and OFCE estimators [see Figs. 6–8(f)]. By comparing Figs. 6–8(c) and Figs. 6–8(e), one can observe that the errors diffuse on larger areas using the OFCE than with our anisotropic version of the OFCE. This is more remarkable in Fig. 8(e), where it is obvious that the error areas in red (bottom left part of the image), blue (bottom middle), and yellow (middle) are much larger with the OFCE. The differences (ANISO–OFCE) in

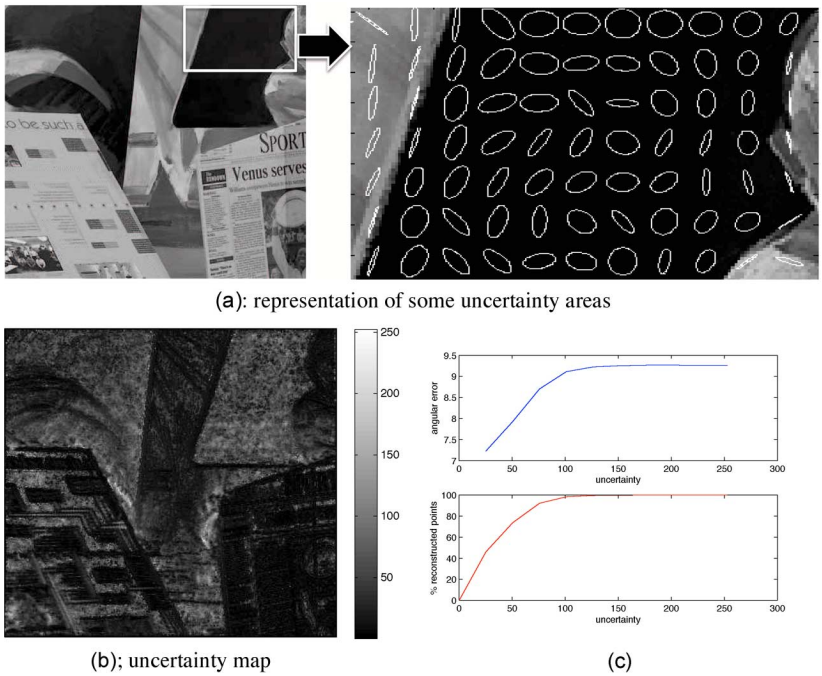

Fig. 9. Uncertainty areas for the Venus sequence. (a) Snapshot of some anisotropic uncertainty areas highlighted by the ANISO technique, in which one can observe that the optical flow is computed depending on the photometric level lines of the luminance. (b) Extracted uncertainty map σ_η. (c) Evolution of the error and percentage of correct motion fields when one takes into account only velocity fields with smaller values of $\sqrt{\sigma_\eta^2 + \sigma_\tau^2}$.

Figs. 6–8(f) highlight the areas where the proposed estimator significantly differs from the OFCE. As expected, the benefit appears in areas where the luminance exhibits high discontinuities, whereas homogeneous areas generate more or less the same behavior of both estimators.

Let us also remember that the motion estimation technique that has been developed for comparing the models of luminance is quite simple (based on the LK estimator). Therefore, as expected, the errors are mainly localized on discontinuities. Since the Venus sequence contains more discontinuity areas than the Dimetrodon one, our results are less performing on this pair of images. However it is very informative to observe that, despite the simplicity of this technique, our results in Table II are very competitive and sometimes outperform advanced dense techniques with a specific process for motion discontinuity recovery. Apart from regions exhibiting motion discontinuities and where the error can be important, the difference fields of Figs. 6(c) and 8(c) reveal very good results (white areas) in the other locations. This suggests that the luminance models introduced in this paper is useful in allowing a global improvement of accuracy.

In addition to the estimated motion fields, such a technique is able to extract the associated uncertainty areas. For each location of the image, these areas represent local neighboring, where the brightness consistency assumption is likely to hold and on which the motion is locally estimated. We have plotted in Figs. 7(a) and 9(a), for a given location of the image, such anisotropic areas, which, in practice, were computed with relations (19) and (23). As one can observe, they correspond to the main structures of the image (mainly anisotropic along the contour and more isotropic in homogeneous regions) and thus provide the user valuable information. Therefore, in a step forward, these areas can be taken into account in a more advanced motion estimation technique in order to better preserve the discontinuities.

The norms of global uncertainty $\sqrt{\sigma_\eta^2 + \sigma_\tau^2}$ maps obtained at the end of the process with the best estimator (the anisotropic one) are plotted in Figs. 7(b) and 9(b). As expected, homogeneous areas where the aperture problem holds correspond to high values of σ_η, whereas small values are linked to photometric contours. Such output of our method is very promising since it highlights the main structures of the images and gives an indicator of the quality of the estimation. To justify this last point, we have depicted in Figs. 7(c) and 9(c) the reconstructed errors when we take into account for the evaluation only the points where the incertitude is below a given value (blue lines) and the corresponding percentage of points used for the computation (red lines). In the two cases, the error grows with the uncertainty, which indicates that it is a reliable indicator of the quality of the measurements.

We then strongly believe that the stochastic models presented can be exploited in the future to design dense estimators relying on the proposed brightness consistency model.

Let us now turn to some experiments on the complete Middlebury database.

Evaluation on the complete database: In a second step, we have applied the proposed local estimator in its anisotropic version (since it performs better on images with the ground truth) on the evaluation data set. A snapshot of numerical results is depicted in Fig. 10. Our method is named "SLK" for stochastic LK. One can observe that the presented technique is the best in the category of "local estimators" since it outperforms the pyramid LK and the FOLKI estimator, this latter being based on a local window registration [17]. In addition, it is promising to observe that it is more efficient than some dense techniques,

Average angle error	avg. rank	Army (Hidden texture) GT all	Army im0 all	Army im0 disc	Army im0 untext	Army im1 all	Army im1 disc	Army im1 untext	Mequon (Hidden texture) GT all	Mequon im0 all	Mequon im0 disc	Mequon im0 untext	Mequon im1 all	Mequon im1 disc	Mequon im1 untext	Schefflera (Hidden texture) GT all	Schefflera im0 all	Schefflera im0 disc	Schefflera im0 untext	Schefflera im1 all	Schefflera im1 disc	Schefflera im1 untext	Wooden (Hidden texture) GT all	Wooden im0 all	Wooden im0 disc	Wooden im0 untext	Wooden im1 all	Wooden im1 disc	Wooden im1 untext	Grove (Synthetic) GT all	Grove im0 all	Grove im0 disc	Grove im0 untext	Grove im1 all	Grove im1 disc	Grove im1 untext	Urban (Synthetic) GT all	Urban im0 all	Urban im0 disc	Urban im0 untext	Urban im1 all	Urban im1 disc	Urban im1 untext	Yosemite (Synthetic) GT all	Yosemite im0 all	Yosemite im0 disc	Yosemite im0 untext	Yosemite im1 all	Yosemite im1 disc	Yosemite im1 untext	Teddy (Stereo) GT all	Teddy im0 all	Teddy im0 disc	Teddy im0 untext	Teddy im1 all	Teddy im1 disc	Teddy im1 untext
SLK [50]	46.0	11.6 47	26.0 50	14.6 48	15.3 46	25.0 49	17.5 47	17.8 47	30.1 48	18.1 47	25.4 51	33.6 49	28.0 51	5.25 48	5.90 46	7.03 49	10.3 49	27.4 50	10.6 49	2.89 24	4.47 31	2.94 31	14.9 49	20.7 49	18.8 49
Adaptive flow [47]	46.8	13.2 48	20.8 45	14.0 47	17.1 48	22.0 44	17.9 48	18.1 48	27.1 44	22.8 51	11.8 43	31.1 45	10.5 43	6.35 50	7.13 50	6.25 48	9.87 48	21.8 44	9.44 47	12.6 51	11.4 51	20.0 51	7.75 44	13.6 41	7.73 43
FOLKI [16]	48.5	10.5 46	25.6 49	11.9 46	20.9 50	26.2 50	26.1 50	17.6 45	31.1 50	16.5 44	15.4 47	32.6 47	16.0 47	6.16 49	6.53 49	9.07 50	12.2 50	29.7 51	13.0 50	4.67 47	5.83 47	9.41 49	18.2 50	22.8 50	25.1 50
Pyramid LK [2]	49.9	13.9 50	20.9 46	21.4 51	24.1 51	23.1 45	30.2 51	20.9 51	29.5 47	21.9 50	22.2 50	34.6 50	25.0 50	18.7 51	23.1 51	20.2 51	21.2 51	24.5 49	21.0 51	6.41 50	7.02 49	10.8 50	25.6 51	31.5 51	34.5 51

Fig. 10. Results on the Middlebury database quantitative values of the evaluation data set. One can observe that our method (SLK) is better than other local estimators (pyramid LK and FOLKI).

such as the one named "Adaptive flow" with adaptive smoothness priors.

Of course, its efficiency is poorer than sophisticated optical flow approaches equipped with advanced smoothing terms since only a coarse estimation corresponding to uncertainty level $\sigma^{\ell}_{\min}$ is available (without any smoothing). Therefore, all discontinuities are completely smoothed out. Nevertheless, these experiments prove that the introduction of uncertainty models in the data term enhances the quality of the estimation since comparable local estimators based on the OFCE are less competitive. To enforce the relevance of the observation model, we should note that, on sequences where the flow possesses softer discontinuities such as Yosemite or Dimetrodon, the quality grows and outperforms several dense methods. All results can be seen in the Middleburry web site.[2]

VI. Conclusion

In this paper, an observation model for optical flow estimation has been introduced. The new operator is based on stochastic modeling of the brightness consistency uncertainty. This data model constitutes a natural extension of the usual brightness consistency assumption. Isotropic and anisotropic uncertainty models have been presented. From this new data term, we have designed a simple local motion estimator where the multiresolution is also interpreted in terms of a spatial uncertainty.

The performances of this local estimator have been validated on synthetic fluid flows issued from DNSs and on the Middleburry synthetic database. In the first case, the results have exhibited significant performances, particularly in the recovery of small scales that are generally smoothed out by spatial regularizers of dense approaches. As for the Middleburry database, the simple local implementation of the presented data term outperforms local approaches. We therefore believe that this stochastic modeling is a very promising alternative to the usual deterministic OFCE for all optical flow methods.

Appendix

Conditional expectation given $\boldsymbol{X}_{t-1}$ of any function $\Psi(\boldsymbol{X}_t, t)$ of a stochastic process defined through Itô diffusion (3) and discretized through an Euler scheme $\boldsymbol{X}_t = \boldsymbol{X}_{t-1} + \boldsymbol{v}(\boldsymbol{X}_{t-1})dt + \boldsymbol{\Sigma}^{1/2}(B_{t+1} - B_t)$ may be written as

$$E\left(\Psi(\boldsymbol{X}_t, t)|\boldsymbol{X}_{t-1}\right) = \int_{\mathbb{R}} \Psi(\boldsymbol{X}_t, t) p(\boldsymbol{X}_t|\boldsymbol{X}_{t-1}) d\boldsymbol{X}_t. \quad (28)$$

[2]http://vision.middlebury.edu/flow/eval/results/results-e1.php

As process $\boldsymbol{X}_t$ is known up to Brownian motion $\boldsymbol{\Sigma} d\boldsymbol{B}_t$, probability $p(\boldsymbol{X}_t|\boldsymbol{X}_{t-1})$ is a multidimensional Gaussian of variance $\boldsymbol{\Sigma}\sqrt{dt}$ ($dt = 1$ here), and we get

$$\begin{aligned} E\left(\Psi(\boldsymbol{X}_t)|\boldsymbol{X}_{t-1}\right) = & \frac{1}{\sqrt{2\pi}\det(\boldsymbol{\Sigma})^{\frac{1}{2}}} \int_{\mathbb{R}} \Psi(\boldsymbol{X}_t, t) \\ & \cdot \exp\Big(-(\boldsymbol{X}_{t-1} + \boldsymbol{v} - \boldsymbol{X}_t)\boldsymbol{\Sigma}^{-1} \\ & \cdot (\boldsymbol{X}_{t-1} + \boldsymbol{v} - \boldsymbol{X}_t)\Big) d\boldsymbol{X}_t. \quad (29) \end{aligned}$$

By a change of variable $\mathbf{Y}_t = \boldsymbol{X}_{t-1} + \boldsymbol{v} - \boldsymbol{X}_t$, this expectation can be written as

$$\begin{aligned} E(\Psi(\boldsymbol{X}_t, t)|\boldsymbol{X}_{t-1}) = & \frac{1}{\sqrt{2\pi}\det(\boldsymbol{\Sigma})^{1/2}} \int_{\mathbb{R}} \Psi(\boldsymbol{X}_{t-1} + \boldsymbol{v} - \mathbf{Y}_t, t) \\ & \cdot \exp\left(-\mathbf{Y}_t\boldsymbol{\Sigma}^{-1}\mathbf{Y}_t\right) d\mathbf{Y}_t \\ = & \Psi(\boldsymbol{X}_{t-1} + \boldsymbol{v}, t) * \mathcal{N}(0, \boldsymbol{\Sigma}). \quad (30) \end{aligned}$$

References

[1] E. Arnaud, E. Mémin, and B. Cernuschi-Frias, "Conditional filters for image sequence based tracking—Application to point tracking," *IEEE Trans. Image Process.*, vol. 14, no. 1, pp. 63–79, Jan. 2005.

[2] S. Baker, D. Scharstein, J. Lewis, S. Roth, M. Black, and R. Szeliski, "A database and evaluation methodology for optical flow," in *Proc. ICCV*, 2007, pp. 1–8.

[3] J. L. Barron, D. J. Fleet, and S. S. Beauchemin, "Performance of optical flow techniques," *Int. J. Comput. Vis.*, vol. 12, no. 1, pp. 43–77, Feb. 1994.

[4] F. Becker, B. Wieneke, S. Petra, A. Schröder, and C. Schnörr, "Variational adaptive correlation method for particle image velocimetry," *IEEE Trans. Image Process.*, 2011, to be published.

[5] M. Black and P. Anandan, "Robust incremental optical flow," Proc. Conf. Comput. Vis. Pattern Recog. J. Eklundh, Ed. New York, Springer-Verlag, 1992, vol. 800, LNCS, pp. 296–302.

[6] T. Brox, A. Bruhn, N. Papenberg, and J. Weickert, "High accuracy optical flow estimation based on a theory for warping," in *Proc. ECCV*, 2004, pp. 25–36.

[7] A. Bruhn, J. Weickert, T. Kohlberger, and C. Schnörr, "A multigrid platform for real-time motion computation with discontinuity-preserving variational methods," *Int. J. Comput. Vis.*, vol. 70, no. 3, pp. 257–277, Dec. 2006.

[8] C. Cassisa, S. Simoens, and V. Prinet, "Two-frame optical flow formulation in an unwarping multiresolution scheme," in *Proc. 14th Iberoamerican Conf. Pattern Recog. (CIARP)*, Guadalajara, Mexico, 2009, vol. 5856, LNCS, pp. 790–797, New York:Springer-Verlag.

[9] T. Corpetti, E. Mémin, and P. Pérez, "Estimating fluid optical flow," in *Proc. Int. Conf. Pattern Recog.*, Barcelona, Spain, Sep. 2000, vol. 3, pp. 1045–1049.

[10] T. Corpetti, E. Mémin, and P. Pérez, "Dense estimation of fluid flows," *IEEE Trans. Pattern Anal. Mach. Intell.*, vol. 24, no. 3, pp. 365–380, Mar. 2002.

[11] J. Fitzpatrick, "The existence of geometrical density-image transformations corresponding to object motion," *Comput. Vis. Graph. Image Process.*, vol. 44, no. 2, pp. 155–174, Nov. 1988.
[12] B. Galvin, B. McCane, K. Novins, D. Mason, and S. Mills, "Recovering motion fields: An analysis of eight optical flow algorithms," in *Proc. Brit. Mach. Vis. Conf.*, Southampton, U.K., 1998, pp. 195–204.
[13] P. Héas, E. Mémin, D. Heitz, and P. Mininni, "Bayesian selection of scaling laws for motion modeling in images," in *Proc. ICCV*, Kyoto, Japan, Oct. 2009, pp. 971–978.
[14] D. Heitz, E. Mémin, and C. Schnörr, "Variational fluid flow measurements from image sequences: Synopsis and perspectives," *Exp. Fluids*, vol. 48, no. 3, pp. 369–393, Mar. 2010.
[15] B. Horn and B. Schunck, "Determining optical flow," *Artif. Intell.*, vol. 17, no. 1–3, pp. 185–203, Aug. 1981.
[16] R. Kimmel and A. M. Bruckstein, "Tracking level sets by level sets: A method for solving the shape from shading problem," *Comput. Vis. Image Understand.*, vol. 62, no. 1, pp. 47–58, Jul. 1995.
[17] G. Le Besnerais and F. Champagnat, "Dense optical flow by iterative local window registration," in *Proc. IEEE ICIP*, Sep. 2005, vol. 1, pp. I-137–I-140.
[18] V. Lempitsky, S. Roth, and C. Rother, "FusionFlow: Discrete–continuous optimization for optical flow estimation," in *Proc. IEEE CVPR*, 2008, pp. 1–8.
[19] T. Lindeberg, "Scale-space theory: A basic tool for analysing structures at different scales," *J. Appl. Statist.*, vol. 21, no. 2, pp. 224–270, 1994.
[20] B. Lucas and T. Kanade, "An iterative image registration technique with an application to stereovision," in *Proc. IJCAI*, 1981, pp. 674–679.
[21] A. Mansouri, "Region tracking via level set PDEs without motion computation," *IEEE Trans. Pattern Anal. Mach. Intell.*, vol. 24, no. 7, pp. 947–961, Jul. 2002.
[22] E. Mémin and P. Pérez, "Dense estimation and object-based segmentation of the optical flow with robust techniques," *IEEE Trans. Image Process.*, vol. 7, no. 5, pp. 703–719, May 1998.
[23] H. Nagel, "Extending the oriented smoothness constraint into the temporal domain and the estimation of derivatives of optical flow," in *Proc. 1st Eur. Conf. Comput. Vis.*, Antibes, France, Apr. 1990, pp. 139–148.
[24] P. Nesi, "Variational approach to optical flow estimation managing discontinuities," *Image Vis. Comput.*, vol. 11, no. 7, pp. 419–439, Sep. 1993.
[25] B. Oksendal, *Stochastic Differential Equations*. New York: Spinger-Verlag, 1998.
[26] N. Papadakis, T. Corpetti, and E. Mémin, "Dynamically consistent optical flow estimation," in *Proc. IEEE ICCV*, Oct. 2007, pp. 1–7.
[27] N. Papadakis and E. Mémin, "A variational technique for time consistent tracking of curves and motion," *J. Math. Imaging Vis.*, vol. 31, no. 1, pp. 81–103, May 2008.
[28] N. Papenberg, A. Bruhn, T. Brox, S. Didas, and J. Weickert, "Highly accurate optic flow computation with theoretically justified warping," *Int. J. Comput. Vis.*, vol. 67, no. 2, pp. 141–158, Apr. 2006.
[29] N. Paragios and R. Deriche, "Geodesic active regions: A new framework to deal with frame partition problems in computer vision," *J. Vis. Commun. Image Represent.*, vol. 13, no. 1/2, pp. 249–268, Mar. 2002.
[30] B. Schunck, "The image flow constraint equation," *Comput. Vis. Graph. Image Process.*, vol. 35, no. 1, pp. 20–46, Jul. 1986.
[31] C. Tomasi and T. Kanade, Detection and tracking of points features School Comput. Sci., Carnegie Mellon Univ., Pittsburgh, PA, Tech. Rep. CMU-CS-91-132, Apr. 1991.
[32] O. Tretiak and L. Pastor, "Velocity estimation from image sequences with second order differential operators," in *Proc. 7th Int. Conf. Pattern Recog.*, Montreal, QC, Canada, 1984, pp. 16–19.
[33] J. Weber and J. Malik, "Robust computation of optical flow in a multi-scale differential framework," *Int. J. Comput. Vis.*, vol. 14, no. 1, pp. 67–81, Jan. 1995.
[34] A. Wedel, T. Pock, J. Braun, U. Franke, and D. Cremers, "Duality TV-L1 flow with fundamental matrix prior," in *Proc. Image Vis. Comput.*, Auckland, New Zealand, Nov. 2008.
[35] J. Weickert and C. Schnörr, "Variational optic-flow computation with a spatio-temporal smoothness constraint," *J. Math. Imaging Vis.*, vol. 14, no. 3, pp. 245–255, May 2001.
[36] Y. Wu, T. Kanade, C. Li, and J. Cohn, "Image registration using wavelet-based motion model," *Int. J. Comput. Vis.*, vol. 38, no. 2, pp. 129–152, Jul. 2000.
[37] L. Xu, J. Chen, and J. Jia, "A segmentation based variational model for accurate optical flow estimation," in *Proc. Eur. Conf. Comput. Vis.*, 2008, pp. I: 671–I: 684.
[38] J. Yuan, C. Schnörr, and E. Mémin, "Discrete orthogonal decomposition and variational fluid flow estimation," *J. Math. Imaging Vis.*, vol. 28, no. 1, pp. 67–80, May 2007.

Thomas Corpetti received the Ph.D. degree in computer vision and applied mathematics and the Habilitation degree from the University Rennes I, Rennes, France, in 2002 and 2011, respectively.

After completing his doctoral work, he spent one year as an Assistant Professor with the University Rennes I and one year as a Postdoctoral Fellow with Cemagref, which is an environment institute. He then obtained a permanent Researcher position with the French National Institute for Scientific Research (CNRS) in 2004 on the analysis of remote sensing image sequences for environmental applications. Since 2009, he has been with the Sino-French Laboratory on Computer Sciences, Automatics and Applied Mathematics (LIAMA), Institute of Automation, Chinese Academy of Sciences, Beijing, China. Since 2010, he has been heading the Turbulence, Images, Physics and Environment Group. His main research interests are concerned with the definition of computer vision tools for the analysis of remote sensing data (low and high resolution) for environmental applications. He is particularly involved in fluid motion analysis/estimation, data assimilation, and change detection projects.

Etienne Mémin received the Ph.D. and Habilitation degrees from the University Rennes I, Rennes, France, in 1993 and 2003, respectively.

He was an Assistant Professor with the University of Bretagne Sud, Morbihan, France, from 1994 to 1999. From September 2001 to September 2003, he was on secondment at the French National Institute for Scientific Research (CNRS). From 2003 to 2007, he headed a "Future and Emerging Technology" basic research European project entitled FLUID. From 2006 to 2008, he was on an invited research position with the University of Buenos Aires, Buenos Aires, Argentina. He is currently affiliated with the National Institute for Research in Computer Science and Control (INRIA), Rennes, where he holds a position of Director of Research. He is heading the Fluminance Group, which is jointly affiliated with Cemagref and INRIA. He principally does his research in the field of fluid motion analysis from image sequences. This essentially concerns the study of methodologies for the estimation or tracking along time of characteristic features transported by fluid flows and observed through image sequences. The direct use of computer vision techniques built from generic luminance conservation laws and rigid body (or weakly deformable) assumptions is generally not appropriate in this context. We thus aim at devising estimation techniques that take more properly into account the dynamics or physics of the observed phenomena. These issues are formulated within either variational or stochastic frameworks. This research activity is at the crossing of several disciplines such as geophysical sciences, fluid mechanics, computer vision, and applied Mathematics.